

General Relativistic, Neutrino-Assisted MHD winds - Theory and Application to GRBs. I. Schwarzschild Geometry

Amir Levinson¹

ABSTRACT

A model for GRMHD disk outflows with neutrino-driven mass ejection is developed, and employed to calculate the structure of the outflow in the sub-slow magnetosonic region and the mass loading of the outflow, under conditions anticipated in the central engines of gamma-ray bursts. The dependence of the mass flux on the conditions in the disk, on magnetic field geometry, and on other factors is carefully examined for a range of neutrino luminosities expected in hyperaccreting black holes. It is found that a fraction of up to a few percent of the neutrino luminosity produced inside the disk is deposited in the upper disk layers, resulting in a steep rise of the specific entropy and the consequent ejection of baryons along magnetic field lines. For the range of conditions explored the final value of the dimensionless entropy per baryon in the wind is typically below 100. The fraction of neutrino luminosity that is ultimately being converted to kinetic energy flux is shown to be a sensitive function of the effective neutrino temperature at the flow injection point, and the shape of magnetic field lines in the sub-slow region, but is practically independent of the strength of poloidal and toroidal magnetic fields. We conclude that magnetic launching of ultra-relativistic polar outflows from the innermost parts of the disk is in principle possible provided the neutrino luminosity is sufficiently low, $L_\nu \lesssim 10^{52}$ erg s⁻¹ or so. The conditions found to be optimal for the launching of an ultra-relativistic jet are also the conditions favorable for large neutron-to-proton ratio in the disk, suggesting that a large neutron excess in GRB jets, as often conjectured, may be possible. However, the outflow time appears to be comparable to the neutronization timescale, implying that the electron fraction should evolve during the initial acceleration phase. Further analysis is required to determine the composition profile in the wind.

Subject headings: accretion, accretion disks - gamma rays: bursts - MHD - relativity - nuclear reactions, nucleosynthesis, abundances

1. Introduction

The central engines that power gamma-ray bursts (GRBs) are thought to consist of a newly formed stellar mass black hole surrounded by a hot, dense, magnetized disk. The prompt and afterglow emissions are inferred to be produced in ultra-relativistic outflows that are launched by the central engine and accelerate to Lorentz factors $\gamma_\infty > 100$. The free energy source of those relativistic, gamma-ray emitting jets can be either the gravitational potential energy of accreted matter or the spin energy of a Kerr black hole. Whether due to dissipation of some fraction of the spin energy of the hole (van Putten & Levinson 2003; Levinson 2005), or owing to hyper-accretion rates (Popham et al. 1999; Pruet et al. 2003), the disk

¹School of Physics & Astronomy, Tel Aviv University, Tel Aviv 69978, Israel; Levinson@wise.tau.ac.il

surrounding the black hole is expected to be sustained at MeV temperatures, and its midplane density is expected to be high, in excess of $10^{10} \text{ gr cm}^{-3}$. Under such conditions the disk is optically thick to electromagnetic radiation and the dominant energy loss mechanism is neutrino emission. Additionally, the nuclear composition in the inner parts of the disk is likely to be neutron rich (Beloborodov, 2003; Pruet et al. 2003); the neutron-to-proton ratio can in principle approach 30 if the disk material is cold enough ($T \gtrsim 2 \text{ MeV}$) and dense enough ($\rho \gtrsim 10^{11} \text{ gr cm}^{-3}$ at the disk midplane; see e.g., fig. 1 in Beloborodov [2003]). The prodigious neutrino luminosity is expected to drive a powerful wind from the disk. This wind is most likely baryon rich and expands at sub or mildly relativistic speeds except, perhaps, inside a core containing the putative baryon poor GRB jet. The surrounding baryon rich wind may play an important role in the collimation of the central jet (Levinson & Eichler, 2000; Rosswog & Ramirez-Ruiz, 2003), and its presence may also lead to some observational consequences (e.g., a supernova-like event). The nuclear composition of the disk outflow, particularly the central GRB jet, is an issue of considerable interest. If, as often assumed, the GRB jet picks up nuclei from the disk (e.g., Derishev, Kocharovsky & Kocharovsky 1999; Beloborodov 2003) then it may contain matter with a large neutron excess that is likely to affect its dynamics (Fuller et al. 2000; Vlahakis, Peng & Konigl 2003; Rossi et al. 2005), as well as some of the characteristics of the afterglow emission (e.g., Derishev, Kocharovsky & Kocharovsky 1999; Bachall & Meszaros 2000). In addition, the disk wind may be a potential site for nucleosynthesis (Pruet et al. 2004, 2005). The nuclear composition of the disk outflow should depend on the conditions at the disk surface and the details of mass ejection process, particularly on the ratio of outflow time and neutronization timescale.

The gross features of the physical picture outlined above are supported by recent numerical simulations (e.g., Proga et al. 2003; McKinney, 2005a; and references therein), however, the detailed structure and properties of the polar outflow are only marginally resolved. In particular, the origin of the fireball - whether emanates from the inner regions of the disk or produced via a BZ mechanism, the nature of the baryon loading process, and the nuclear composition of the outflow are yet open issues. Moreover, as will be shown below the mass ejection process is rather sensitive to the conditions at the flow injection point and the physical processes involved, which makes it difficult to study using global numerical simulations.

In order that a wind be accelerated hydrodynamically to high Lorentz factors, the entropy per baryon at the wind injection region must be extremely high. Purely hydrodynamic fireballs demand $s/k_B \gtrsim 10^5 (\gamma_\infty/200)(kT_d/2\text{MeV})^{-1}$ where γ_∞ is the terminal Lorentz factor of the fireball and T_d is the temperature at the base of the outflow. Although the specific entropy of the fireball should rise as it accelerates, owing to absorption of neutrinos escaping from the dense layers of the disk, such extreme values are unlikely to be achieved. The requirements on the baryon loading can be alleviated if the outflow is magnetically dominated. In that case, the disk must support an ordered magnetic field with strength in excess of a few times 10^{14} G to account for the observed GRB energies (e.g., Levinson & Eichler 1993; Meszaros & Rees, 1997). Such strong fields conceivably exist in the dense disks of hyperaccreting black holes (e.g., McKinney, 2005b). Since the energy is extracted magnetically, acceleration of the outflow to high Lorentz factors does not require, in principle, high specific entropy, but rather a high magnetic energy per baryon \mathcal{E}_B . In the ideal MHD case $\mathcal{E}_B > \gamma_\infty \sim 200$ and if the fireball accelerates along magnetic field lines that are anchored to the disk, the question then arises as to how baryon overloading of magnetic field lines can be avoided. Vlahakis, Peng & Konigl (2003) proposed that such high \mathcal{E}_B may not in fact be necessary if the ratio of baryon-to-magnetic flux is not conserved on magnetic flux surfaces. Specifically, they considered a situation in which a neutron rich outflow, expelled along magnetic field lines that emanate from accreted disk material in the vicinity of the innermost stable circular orbit, is accelerated magnetically to a Lorentz factor of order 10, at which point the neutrons decouple. The remaining protons then continue to accelerate magnetically to $\gamma_\infty \sim 200$. With n/p ratio of about 30, $\mathcal{E}_B \sim 10$ or so is sufficient before decoupling (but

not smaller, otherwise the neutrons wont decouple at all). However, such a high n/p ratio requires optimal conditions in the disk, and essentially no evolution of the electron fraction Y_e during the acceleration phase prior to decoupling, which is questionable.

The issue of mass loading has not been addressed in most of the previous work on magnetized, relativistic disk outflows. The common approach, following the pioneering work of Blandford & Payne (1982), is to seek self-similar solutions of the trans-field equation (Li et al., 1992; Contopoulos 1994; Vlahakis & Konigle 2003). While such a treatment considerably simplifies the analysis, it precludes the incorporation of gravity (in the relativistic case) as well as neutrino heating in the flow equations, and in addition does not allow matching of the self-similar outflow solution to a Keplerian disk (Li et al. 1992). The immediate implication is that the self-similar outflow solutions cannot be extended down to the sub-slow magnetosonic region. On the other hand, the mass-to-magnetic flux ratio is determined by the regularity condition at the slow magnetosonic point, namely by the requirement that the outflow must pass smoothly through this point. This means that solutions of the flow equations in the sub-slow magnetosonic region must be obtained in order for the mass flux to be calculated. Since the self-similar treatment is inapplicable in this region, one must seek a different approach. In this paper we construct a model for GRMHD disk outflows with neutrino-driven mass ejection, and employ it to calculate the structure of the flow in the sub-slow region. Using the regularity condition at the slow magnetosonic point we carefully examine how the mass flux depends on the conditions at the injection point, on geometry of magnetic surfaces, and on other wind quantities. In §2 we present the basic equations for a GRMHD wind with external energy and momentum sources. In §3 we derive analytic expressions for the flow quantities in terms of the location and temperature at the slow point by employing the regularity condition, and identify some systematic trends. In §4 we present numerical solutions. Our approach is to integrate the flow equations assuming the magnetic field geometry is given. Since the slow point is located close to the disk midplane, our choice of a particular field geometry reflects in part a choice of boundary conditions. We explore a range of field geometries in order to elucidate the dependence of the mass flux on the shape of the field lines.

Neutrino-driven winds have been discussed previously in other contexts (e.g., Duncan et al. 1986; Levinson & Eichler 1993; Woosley et al. 1994; Witt et al. 1994; Qian & Woosley 1996; Thompson et al. 2001). However, most previous models assume purely hydrodynamic, spherically symmetric winds, which are less relevant to the problem at hand. A simplified model of hydrodynamic disk outflow is presented in Pruet et al. (2004), mainly in connection with nucleosynthesis. In this work we generalize those previous treatments to incorporate GRMHD effects and disk geometries.

2. GRMHD Neutrino-Assisted Wind Model

We consider a MHD wind expelled from the surface of a hot, magnetized disk surrounding a non-rotating black hole. The range of conditions in the disk is envisioned to be similar to that computed by Popham et. al. (1999) for hyperaccreting black holes with mass accretion rates $10^{-1} - 10 M_\odot \text{ s}^{-1}$ and viscosity parameters $\alpha_{vis} = 0.01 - 0.1$. Under such conditions the total neutrino luminosity emitted from the disk lies in the range $L_\nu = 10^{51} - 10^{54} \text{ erg s}^{-1}$. We focus our attention on the inner regions of the disk (within 10 Schwarzschild radii or so) where the midplane density exceeds about 10^9 gr cm^{-3} , and where the major fraction of the neutrino luminosity is generated.

Now, for the range of temperatures considered the torus material should be a mixture of baryons and a light fluid (photons and electron-positron pairs in equilibrium). The light and baryonic fluids will be

tightly coupled in the sub-slow magnetosonic region, owing to the large Thomson depth. Deep beneath its surface, the torus is in a hydrostatic equilibrium where the vertical gravitational force exerted on it by the black hole is supported by the baryon pressure. In this region heating and cooling processes due to neutrino emission and absorption proceed at very high rates, and the temperature variation in the vertical direction is expected to be very small. As a consequence, the vertical density profile is roughly a Gaussian with a rather small scale height ($h/R_0 \lesssim 0.1$; see below). As the density drops, the ratio of light fluid pressure to baryonic pressure increases roughly as T^3/ρ , until at $\rho \lesssim 10^8 T_{MeV}^3 \text{ gr cm}^{-3}$ the light fluid pressure dominates over the baryonic pressure (see eq. [23] below). At this point hydrostatic equilibrium can no longer be sustained and the matter starts accelerating along magnetic field lines. This suggests that the mass flux carried by the wind should be controlled by the heating and cooling processes at the base of the wind. These processes are therefore incorporated into the flow equations derived below. To simplify the analysis we consider, in what follows, only time independent, axisymmetric models. As shown by Vlahakis & Konigle (2003b), a relativistic MHD pulse can be adequately described by the same equations.

2.1. Basic equations

Since, as explained above, the light and baryonic fluids will be tightly coupled at the base of the outflow, they can be treated as a single fluid. We denote by ρ , p , e , $h = (e + p)/\rho c^2$, the proper baryon rest mass density, total pressure, total energy density, and dimensionless specific enthalpy of this mixed fluid. The stress-energy tensor then takes the form:

$$T^{\alpha\beta} = h\rho c^2 u^\alpha u^\beta + pg^{\alpha\beta} + \frac{1}{4\pi}(F^{\alpha\sigma} F_\sigma^\beta - \frac{1}{4\pi}g^{\alpha\beta} F^2), \quad (1)$$

where u^α is the four-velocity measured in units of c , $F_{\mu\nu} = \partial_\mu A_\nu - \partial_\nu A_\mu$ is the electromagnetic tensor, and $g^{\alpha\beta}$ is the metric tensor. In what follows we take spacetime to have a Schwarzschild geometry, defined by the line element $ds^2 = -\alpha^2 dt^2 + \alpha^{-2} dr^2 + r^2 d\theta^2 + R^2 d\phi^2$, with $\alpha^2 = 1 - r_s/r$, and $R = r \sin \theta$. We denote by q^β the source terms associated with energy and momentum transfer by some external agent. The dynamics of the MHD system is then governed by the following set of equations: energy and momentum equations

$$\frac{1}{\sqrt{-g}}(\sqrt{-g}T^{\alpha\beta})_{,\alpha} + \Gamma^\beta_{\mu\nu} T^{\mu\nu} = q^\beta, \quad (2)$$

continuity equation

$$\frac{1}{\sqrt{-g}}(\sqrt{-g}\rho u^\alpha)_{,\alpha} = 0, \quad (3)$$

and Maxwell's equations,

$$F_{;\alpha}^{\beta\alpha} = \frac{1}{\sqrt{-g}}(\sqrt{-g}F^{\beta\alpha})_{,\alpha} = 4\pi j^\beta, \quad (4)$$

$$F_{\alpha\beta,\gamma} + F_{\beta\gamma,\alpha} + F_{\gamma\alpha,\beta} = 0. \quad (5)$$

We assume the flow to be stationary and axisymmetric ($\partial_t = \partial_\phi = 0$), and require infinite conductivity, $u^\alpha F_{\alpha\beta} = 0$. The above set of equations then admit two invariants: the mass-to-magnetic flux ratio

$$\eta = \frac{\rho u_p}{B_p} \quad (6)$$

and the angular velocity,

$$\Omega = v^\phi - \frac{\eta}{\sqrt{-g}\rho u^t} F_{r\theta} = v^\phi - \frac{v_p}{B_p} \frac{B_\phi}{R}. \quad (7)$$

Here u_p is the poloidal 4-velocity of the fluid defined by $u_p^2 = u^r u_r + u^\theta u_\theta$, $v_p = u_p/\gamma$ is the corresponding 3-velocity, where $\gamma = \alpha u^t$ is the Lorentz factor, $v^\phi = u^\phi/u^t$, B_p is a rescaled poloidal magnetic field defined through $B_p^2 = (B^r B_r + B^\theta B_\theta)/\alpha^2$, and $B_\phi = r F^{r\theta}/\alpha$ is the toroidal magnetic field. By contracting u_β with eq. (2), using the identity $\Gamma_{\mu\nu}^\beta u_\beta u^\mu u^\nu = -u_\beta u^\nu (u^\beta)_{,\nu}$, and the thermodynamic identity $dh = dp/\rho c^2 + (k_B T/m_N c^2) ds$, where s is the dimensionless specific entropy and m_N is the nucleon rest mass, we obtain the change in s along magnetic flux surfaces:

$$(\rho/m_N) k_B T u^\alpha s_{,\alpha} = -u_\alpha q^\alpha. \quad (8)$$

By contracting $g_{\beta\gamma}$ with eq. (2) and taking the t and ϕ components, we obtain

$$\rho c^2 u^\alpha \mathcal{E}_{,\alpha} = -q_t, \quad (9)$$

$$\rho c^2 u^\alpha \mathcal{L}_{,\alpha} = q_\phi, \quad (10)$$

where

$$\mathcal{E} = -h u_t - \frac{\sqrt{-g}}{4\pi\eta c^2} \Omega F^{r\theta} = h\gamma\alpha - \frac{\alpha R \Omega B_\phi}{4\pi\eta c^2}, \quad (11)$$

and

$$\mathcal{L} = h u_\phi - \frac{\sqrt{-g}}{4\pi\eta c^2} F^{r\theta} = h u_\phi - \frac{\alpha R B_\phi}{4\pi\eta c^2}, \quad (12)$$

are the specific energy and angular momentum of the MHD system, respectively. We henceforth assume that $q_\phi = 0$, so that the specific angular momentum is conserved. By employing eqs (6) (7) (11) (12) we can express the toroidal magnetic field in terms of the flow parameters:

$$B_\phi = -\frac{4\pi\eta}{\alpha R} \frac{\alpha^2 \mathcal{L} - R^2 \Omega \mathcal{E}}{(\alpha^2 - R^2 \Omega^2 - M^2)}, \quad (13)$$

where M is the Alfvén Mach number defined by $M^2 = 4\pi h \eta^2 c^2 / \rho = u_A^2 / u_p^2$, with $u_A^2 = B_p^2 / (4\pi h \rho c^2)$. Using eqs (7), (11) and (12), and the normalization condition $u^\alpha u_\alpha = -1$ yields

$$1 + u_p^2 = \frac{(\mathcal{E} - \Omega \mathcal{L})^2 (\alpha^2 - R^2 \Omega^2 - 2M^2) - [(\mathcal{L}/R)^2 - (\mathcal{E}/\alpha)^2] M^4}{h^2 (\alpha^2 - R^2 \Omega^2 - M^2)^2}. \quad (14)$$

We can differentiate eq. (14) along a given stream line to obtain

$$(\ln u_p)' = \frac{N + N_q}{D}, \quad (15)$$

where $(')$ denotes derivative along the stream line $\Psi = \text{const}$, and

$$D = -(\alpha^2 - R^2 \Omega^2 - M^2)^2 (u_p^2 - u_{SM}^2) (u_p^2 - u_{FM}^2) / u_A^2, \quad (16)$$

$$N = \zeta_1 (\ln B_p)' + \zeta_2 (\ln \alpha)' + \zeta_3 (\ln R)', \quad (17)$$

$$N_q = \zeta_4 (\ln \mathcal{E})' + \zeta_5 (\ln s)'. \quad (18)$$

Here u_{SM} and u_{FM} are the slow and fast magnetosonic wave speeds, respectively, and are given in eqs. (A18) and (A19), and c_s is the sound 4-velocity defined by $c_s^2 = a_s^2 / (1 - a_s^2)$ with a_s^2 given in eq. (25) below. The coefficients ζ_i are functions of the flow parameters, viz., $\zeta_i = \zeta_i(\Omega, \mathcal{L}, \mathcal{E}, s, M)$, and are derived in the appendix. Equation (15) generalizes the result derived by Takahashi et al. (1990) to the non-adiabatic case. As seen, energy and momentum exchange with an external agent (i.e., $N_q \neq 0$) formally modifies the conditions at the critical points. However, in practice we find this to be a small correction. As shown

below, the main effect of heating is to enhance the temperature and the specific entropy at the slow point. In cases where the stream function is known, the above set of equations, augmented by an equation of state $h = h(\rho, s)$, can be solved to yield the structure of the flow. The poloidal magnetic field can then be expressed in terms of the stream function. Taking A_ϕ as the stream function $\Psi(r, \theta)$ we obtain,

$$B_p^2 = \frac{r^2 \alpha^2 (\Psi_{,r})^2 + (\Psi_{,\theta})^2}{R^2 r^2 \alpha^2}. \quad (19)$$

2.2. Equation of state

For the range of densities and temperatures considered here, we find that the relativistic particles in the vicinity of the slow magnetosonic point are non-degenerate. The total kinetic pressure of the mixed fluid is then given by $p = p_l + p_b$, where

$$p_l = \frac{11}{12} a T^4 = 1.2 \times 10^{26} T_{MeV}^4, \quad \text{dyn cm}^{-2} \quad (20)$$

is the light fluid pressure, and

$$p_b = \rho \frac{kT}{m_N} \simeq 9 \times 10^{26} \rho_9 T_{MeV} \quad \text{dyn cm}^{-2} \quad (21)$$

is the pressure contributed by the baryons, with T_{MeV} being the temperature in MeV units, and ρ_9 the rest mass density in units of 10^9 g cm^{-3} . The dimensionless enthalpy per baryon of the mixed fluid is given by

$$h = 1 + \frac{4p_l}{\rho c^2} + \frac{5}{2} \frac{p_b}{\rho c^2}. \quad (22)$$

It is convenient to define the thermodynamic quantity

$$\sigma = \frac{4p_l}{p_b} = 0.53 \frac{T_{MeV}^3}{\rho_9}. \quad (23)$$

Clearly, the pressure is dominated by the light fluid when $\sigma > 4$. In terms of σ the change in entropy is related to the change in temperature and density through

$$ds = \frac{m_N c^2}{kT} \left(dh - \frac{dp}{\rho c^2} \right) = \left(\frac{3}{2} + 3\sigma \right) \frac{dT}{T} - (1 + \sigma) \frac{d\rho}{\rho}. \quad (24)$$

It is readily seen from eqs (23) and (24) that σ is roughly the entropy per baryon in regions where the light fluid pressure dominates; that is $s \simeq \sigma$ in the limit $\sigma \gg 1$. The relativistic sound speed can now be expressed as:

$$a_s^2 = \left(\frac{\partial \ln h}{\partial \ln \rho} \right)_s = \frac{p_b}{\rho c^2 h} \frac{5 + 10\sigma + 2\sigma^2}{3(1 + 2\sigma)}. \quad (25)$$

We also need the change in h at constant density. Using the above results we obtain

$$\left(\frac{\partial h}{\partial s} \right)_\rho = \frac{kT}{m_N c^2} \frac{5 + 8\sigma}{3(1 + 2\sigma)}. \quad (26)$$

2.3. Rates for neutrino heating and cooling

The neutrino flux emitted from the dense disk layers depends on the structure of and conditions in the disk, which are uncertain. Quite generally the neutrino luminosity comes predominantly from disk radii within a few r_s (Popham et al. 1999). To simplify our calculations, we invoke a spherical neutrino source with a radius $R_\nu = 10^6 R_{\nu 6}$ cm and a total luminosity $L_\nu = 10^{53} L_{\nu 53}$ erg s $^{-1}$, which are treated as free parameters. Some fraction of the energy of the escaping neutrinos is deposited in the surface layers of the disk, via pair neutrino annihilation into electron - positron pairs and neutrino capture on neutrons and protons, thereby giving rise to a significant heating of the matter near the injection point of the wind. It is conceivable that turbulence or magnetic field dissipation may provide additional heating of the surface layers, but these processes are difficult to model and will be ignored. Detailed account of the various neutrino heating and cooling process is given in Qian & Woosley (1996). The heating rate due to neutrino absorption is approximately (see also Bethe and Wilson 1985)

$$\dot{Q}_{\nu n} \simeq 5 \times 10^{31} \frac{L_{\nu 53}^{3/2}}{R_{\nu 6}^3} \rho_9 f_{\nu n}(r) \text{ erg cm}^{-3} \text{ s}^{-1}, \quad (27)$$

and that due to neutrino-antineutrino annihilation into electron-positron pairs is (e.g., Goodman et al. 1987; Qian & Woosley 1996)

$$\dot{Q}_{\nu\bar{\nu}} \simeq 10^{31} \frac{L_{\nu 53}^2}{R_{\nu 6}^4} f_{\nu\nu}(r) \text{ erg cm}^{-3} \text{ s}^{-1}. \quad (28)$$

Here $f_{\nu n}(r) = [1 - (1 - R_\nu^2/r^2)^{1/2}]$, and $f_{\nu\nu}(r) = f_{\nu n}^4(r)[1 - R_\nu^2/r^2 + 4(1 - R_\nu^2/r^2)^{1/2} + 5]$. Energy gain by neutrino capture on nucleons dominates at densities above

$$\rho_9 = 0.2(L_{\nu 53}/R_{\nu 6}^2)^{1/2} (f_{\nu\nu}/f_{\nu n}). \quad (29)$$

As a result of neutrino heating, the surface layers of the disk will quickly rise to temperatures in excess of several Mev, at which emission of secondary neutrinos by the inverse processes; electron and positron capture on nucleons

$$\epsilon_{\nu n} \simeq 10^{27} \rho_9 T_{MeV}^6 \text{ erg s}^{-1} \text{ cm}^{-3}, \quad (30)$$

and electron-positron annihilation into neutrinos

$$\epsilon_{\nu\bar{\nu}} = 5 \times 10^{24} T_{MeV}^9 \text{ ergs s}^{-1} \text{ cm}^{-3}, \quad (31)$$

becomes the dominant energy loss mechanism. Equating the last two rates one obtains the density below which the pair neutrino cooling rate exceeds the cooling rate due to electron and positron capture on nucleons,

$$\rho_9 = 5 \times 10^{-3} T_{MeV}^3. \quad (32)$$

The critical density is found to be always well above this value, implying that URCA cooling is the dominant energy loss mechanism in the regions of interest. The source term associated with energy transfer is given by

$$q^t = \dot{Q}_{\nu n} + \dot{Q}_{\nu\bar{\nu}} - \epsilon_{\nu n} - \epsilon_{\nu\bar{\nu}} \quad (33)$$

Well below the slow-magnetosonic point, where the flow velocity is small and adiabatic cooling is negligible, the temperature profile is determined the condition $q^0 = 0$. In this region the density exceeds the values given by eqs (29) and (32), and so the heating and cooling rates are dominated by capture (eqs. [27] and [30]). The temperature profile is then given to a good approximation by

$$T_{MeV}(r) = 6 \left(\frac{L_{\nu 53}}{R_{\nu 6}^2} \right)^{1/4} f_{\nu n}^{1/6}. \quad (34)$$

3. The Sub-Slow Magnetosonic Region - General Considerations

3.1. The flow near the disk surface

Deep beneath the slow magnetosonic point, the matter is close to hydrostatic equilibrium. Heating and cooling by the neutrinos proceeds at high rates and the temperature is maintained at the level given by eq. (34). If the pressure there is dominated by the baryons, then the density scale height at radius R_0 is roughly $h/R_0 \sim (kT R_0/GMm_p)^{1/2} \simeq 10^{-1.5}(R_0/r_s)^{1/2}T_{MeV}^{1/2}$, which is typically much smaller than unity near the black hole. Consequently, the base of the flow is located close to the disk midplane. Moreover, the ratio of the sound and Alfvén speeds is $c_s/u_A \simeq 10^{-1.5}T_{MeV}^2/B_{p15}$, so that under the conditions envisioned the Alfvén Mach number is anticipated to be very small in the sub-slow region. To order $O(M^2)$ eqs. (A11)-(A13) yield:

$$\zeta_1 = -(\alpha^2 - R^2\Omega^2)^3(1 + u_p^2)c_s^2, \quad (35)$$

$$\zeta_2 = -\frac{\alpha^2(\alpha^2 - R^2\Omega^2)(\mathcal{E} - \Omega\mathcal{L})^2}{(1 - a_s^2)h^2}, \quad (36)$$

$$\zeta_3 = -\zeta_2 \frac{R^2\Omega^2}{\alpha^2}. \quad (37)$$

Consider now a field line described by the equation $R = R(z)$, and denote $R_0 = R(z = 0)$, $R'_0 = dR/dz|_{z=0}$, and $\tilde{N} = (dz/dl)^{-1}N$, where $d/dl = (dz/dl)d/dz$ is the derivative along the field line, and ' denotes now differentiation with respect to z . Close to the disk midplane we can expand $R(z)$ about $z = 0$. To first order in z eq. (17) yields

$$\tilde{N} = \zeta_1(\ln B_p)' + \frac{\zeta_2}{\alpha^2} \{(\Omega_k^2 - \Omega^2)[R_0R'_0 + (R'_0)^2z + R_0R''_0z] + \Omega_k^2[1 - 3(R'_0)^2]z\}, \quad (38)$$

where Ω_k denotes the Keplerian angular velocity at $R = R_0$, viz., $\Omega_k^2 = r_s/2R_0^3$. At the base of the flow adiabatic losses are negligibly small and $N_q \simeq 0$. Now, in reality the poloidal velocity of the outflow should vanish at some height $z_d(R_0)$ above the disk where the streamlines of inflowing matter joins the outflow. At this effective surface the angular velocity Ω is expected to be equal to the local Keplerian angular velocity. To leading order we then find $\Omega^2 = \Omega_k^2(1 - 3R'_0z_d/R_0)$, where the radius at which the field line meets the surface is related to R_0 through $R_d \simeq R_0 + R'_0z_d$. Substituting the latter result into eq. (38) we obtain

$$\tilde{N} = \zeta_1(\ln B_p)' + \frac{\zeta_2}{\alpha^2}\Omega_k^2[z - 3(R'_0)^2(z - z_d)]. \quad (39)$$

From eq. (16) it is evident that $D < 0$ when $u_p < u_{SM}$. Consequently, the condition $N < 0$ must be fulfilled in the sub-slow region in order that the flow be accelerated. If the magnetic field lines are diverging, viz., $(\ln B_p)' < 0$, as one might expect, then the first term on the right hand side of eq. (39) is always positive, implying that the second term must be negative in the sub-slow region. As seen, there are two distinct cases. If the magnetic field lines are inclined at an angle larger than $\pi/6$ to the vertical ($R'_0 > 1/\sqrt{3}$), then the second term on the right hand side of eq. (39) has a root at $z_1 = [3(R'_0)^2/(3(R'_0)^2 - 1)]z_d$ and it changes sign across. Along such field lines the outflow is centrifugally driven and can be initiated even in the cold fluid limit (at which $\zeta_1 = 0$), as was first shown by Blandford & Payne (1982). The slow magnetosonic point is located close to the disk surface, at $z_{sm} \leq z_1$ (the exact location depends on the value of the sound speed at the disk surface). If the magnetic field lines are inclined at an angle smaller than $\pi/6$ to the vertical, then the second term in eq. (39) is negative at $z = 0$ and decreases linearly with z in the region where the above expansion holds. This corresponds to the regime of stable equilibrium, as defined in Blandford & Payne

(1982). Along such field lines the mass flux is thermally driven, similar to the case of a spherical wind. As shown below, the slow magnetosonic point in this case is located on larger scales, $z_{sm} \sim R_0$, where the sound speed roughly equals the escape velocity. The above derivation is in accord with the results obtained by Ogilvie (1997)².

3.2. Conditions at the slow-magnetosonic point

At the critical point $D = 0$ and hence $N + N_q = 0$. Neglecting terms of order M^2 and higher, one finds $u_{SM} = c_s$ and

$$(1 + c_s^2)a_s^2(\ln B_p)' + \frac{\gamma_c^2}{\alpha_c^2}(\alpha_c \alpha_c' - R_c R_c' \Omega^2) - \gamma_c \frac{q^t}{3\rho c^3 u_p} = 0, \quad (40)$$

where eqs (35)-(37) and (A14)-(A16) have been used. Henceforth, subscript c refers to quantities at the critical point. Equation (40) can be solved now for the sound speed a_s . The result can be simplified further by noting that at the slow magnetosonic point the flow is sub-relativistic, so that $c_s^2 \simeq a_s^2 \ll 1$, and $\gamma_c \simeq 1$. Moreover, at the slow point the last term on the LHS of eq. (40) is approximately $q^t/3\rho c^3 u_p \simeq 10^{-9.5} (L_{\nu 53}/R_{\nu 6}^2)^{3/2} (R_{\nu}/r_c)^2 a_s^{-1} \text{ cm}^{-1}$, where eq. (27) has been employed, and can be neglected to lowest order. With the above approximations the solution of eq. (40) reads:

$$a_s^2 = a_{sc}^2 = -\frac{(\alpha_c \alpha_c' - R_c R_c' \Omega^2)}{\alpha_c^2 (\ln B_p)'}. \quad (41)$$

Now, in general we expect $(\ln B_p)' = -A/R_c$, where A is an order unity number, with $A \simeq 2$ for conical flux tubes, $A = 0$ for cylindrical flux tubes, and $A \simeq 1$ in the case of a self-similar magnetic field. In terms of Ω_k eq. (41) can be expressed as:

$$a_{sc}^2 = \frac{R_c}{A} \left\{ \frac{R_c R_c' (\Omega_k^2 R_0^3 - \Omega^2 r_c^3) + \Omega_k^2 z_c R_0^3}{r_c^2 (r_c - r_s)} \right\}, \quad (42)$$

where $r_c^2 = R_c^2 + z_c^2$. From the last equation it is evident that $a_s^2 \ll 1$. Below we find that typically a_s lies in the range $0.1 - 0.01$.

3.2.1. Centrifugally driven mass flow

Since in this case the critical point occurs near the disk surface we can expand $R_c = R(z_c)$ about $z = 0$ as before. Equation (42) then reduces to

$$a_{sc}^2 \simeq \frac{r_s}{R_0 + r_s} \frac{z_c + 3(R_0')^2(z_d - z_c)}{A R_0}. \quad (43)$$

Adopting for illustration $A = 2$, $r_s/R_0 = 0.3$, $z_d/R_0 = 0.1$, we estimate $a_{sc}^2 < 10^{-2}$ at the critical point. Since the latter occurs close to the surface, adiabatic cooling is unimportant and the temperature profile is given to a good approximation by eq. (34). For the range of neutrino luminosities considered here we expect $T_c \gtrsim 1 \text{ MeV}$. The mass loading of the outflow, $\rho_c a_{sc}$, would depend on the density at the flow injection

²Note though that the term $\zeta_1(\ln B_p)'$ is neglected in eq. (5.35) of Ogilvie, which may be justified near the disk surface. However, the omission of this term precludes treatment of transonic outflows along low inclination field lines

point. However, the critical density and, hence, the mass flux cannot be arbitrarily small. To estimate the minimum mass flux, we employ eq. (25) to write

$$a_s^2 = 10^{-3} T_{cMeV} \frac{5 + 10\sigma + 2\sigma^2}{3(1 + 2\sigma)}, \quad (44)$$

and conclude that under the conditions envisioned σ cannot be much larger than unity at the critical point in order for eq. (43) to be satisfied. Equation (23) then implies a critical density of $\rho_c \gtrsim 10^8 T_{cMeV}^3 \text{ g cm}^{-3}$, and a mass flux $\dot{M} \simeq \rho_c a_s \pi R_0^2 > 10^{30} \text{ g s}^{-1}$, for $R_0 = r_s = 10^{6.5} \text{ cm}$. Consequently, outflows along field lines having inclination angles larger than $\pi/6$ are expected to be sub-relativistic, owing to the large mass flux driven from the surface. Numerical integration of the full equations confirms this result.

3.2.2. Thermally driven mass flow

In this case the critical point occurs higher above the disk. As will be shown in sec. 4, the specific entropy rises steeply during the initial acceleration phase, so that $\sigma \gg 1$ near the critical point. Using eqs. (25) and (41) we can relate the critical density to the critical temperature. In the limit $\sigma \gg 1$ we obtain

$$\rho_c \simeq 10^5 \frac{T_{cMeV}^4}{a_{sc}^2} \text{ gr cm}^{-3}. \quad (45)$$

As seen, the critical density is a sensitive function of the critical temperature and, therefore, adiabatic cooling can largely suppress the mass flux. An estimate of the mass-to-magnetic flux ratio can be obtained by noting that the critical point is located roughly at $z_c \sim R_0$, so that $B_{pc} \simeq B_{p0}$. One then finds

$$\eta = \frac{\rho_c c_s}{B_{pc}} \simeq 3 \frac{T_{cMeV}^4}{B_{p015}} a_{sc}^{-1} \text{ gr cm}^{-2} \text{ s}^{-1} \text{ G}^{-1}. \quad (46)$$

From the above result we further estimate that for the range of conditions considered here the relativistic energy per baryon of the matter is dominated by the nucleon rest mass, implying $h_c \gamma_c \alpha_c \simeq 1$. To a good approximation the total energy per baryon (eq. [11]) is then $\mathcal{E} = 1 + \mathcal{E}_B$, with the magnetic energy per baryon given by

$$\mathcal{E}_B \simeq 5 \times 10^2 T_{cMeV}^{-4} B_{p015}^2 a_{sc} \left(\frac{-B_\phi}{B_p} \right)_0. \quad (47)$$

At the highest neutrino luminosities adiabatic cooling can be neglected even along low inclination field lines, and the temperature at the slow point is given to a good approximation by eq. (34) with $r = r_c$. The above quantities can then be estimated once the location of the slow point is known. At lower neutrino luminosities, however, adiabatic cooling will suppress the critical temperature, rendering such estimates highly uncertain. One must then integrate the flow equations in order to accurately compute the location of and temperature at the slow point. This is discussed in the next section.

Equations (41) and (45) imply that, to order $O(M^2)$, the critical mass flux on a given field line, $\rho_c c_s$, depends only on the gravitational potential, the angular velocity, the neutrino luminosity (through the critical temperature T_{cMeV}), and geometry of streamlines, and is independent of the strength of poloidal and toroidal magnetic fields at the disk surface. Consequently, for a given choice of L_ν and magnetic field geometry, there is a critical value of $B_{p0} B_{\phi 0}$ above which $\mathcal{E}_B > 1$ and the flow is essentially magnetically driven. Numerical integration of the flow equation confirms this conclusion, as shown below.

4. Numerical Model

The model outlined above is characterized by three parameters: the black hole mass r_s , the neutrino luminosity L_ν , and the neutrinospheric radius R_ν . Fixing these parameters, eqs. (8), (9) and (15) can be solved simultaneously once the magnetic field geometry is known. In general, however, the stream function is unknown a priori, and one must solve the highly non-linear trans-field equation simultaneously with eqs (8), (9), (22) and (24), and subject to appropriate boundary conditions to fully determine the flow structure. Unfortunately, the inclusion of gravity and external heating breaks scale-freeness, and precludes separation of variables as in self-similar treatments. This means that a self-consistent calculation of the field geometry is impractical. Since in this work we are merely interested in estimating the mass flux driven by neutrino heating it is sufficient to integrate the above flow equations only up to the slow magnetosonic point. As will be shown below, the latter is located rather close to the disk surface where the field geometry should anyhow reflect the boundary conditions. Our approach shall be to specify the stream function and use it to integrate the above set of flow equations along a given field line. We explore different field geometries in order to elucidate the dependence of baryon loading on the basic characteristics of the flux surfaces. The system under consideration has three integrals of motion: The angular velocity Ω , the angular momentum \mathcal{L} , and the mass-to-magnetic flux ratio, η . In our approach, Ω , \mathcal{L} , and the values of \mathcal{E} and B_p at the origin are treated as additional free parameters, and η as an eigenvalue of the system.

In what follows we first describe the magnetic field geometries used in the our calculations.

4.1. Topology of magnetic surfaces

4.1.1. split monopole

In our first example we consider a split monopole field, with its center shifted a distance a from the black hole along the hole rotation axis (see Fig 1). In cylindrical coordinates, the field line equation reads: $R(z) = \kappa(z + a) = \kappa z + R_0$, where $\kappa = \tan \tilde{\theta}$ is the field line parameter and $R_0 = \kappa a$. The stream function has the form $\Psi = \Psi_0(1 - \cos \tilde{\theta})$. Substituting the latter into eq. (19) yields the poloidal magnetic field:

$$\left(\frac{B_p}{B_{p0}}\right)^2 = \frac{\alpha_0^2 R_0^4}{\alpha^2 R^4} \frac{\{(1 + \kappa^2) - r_s R_0^2 (R^2 + z^2)^{-3/2}\}}{(1 + \kappa^2) - r_s/R_0}, \quad (48)$$

where $B_{p0} = B_p(z = 0)$. Note that this geometry implies a current sheet at the disk midplane.

The proper length of a given stream line, measured in units of R_0 , is given by

$$dl = \frac{1}{R_0} (g_{rr} dr^2 + g_{\theta\theta} d\theta^2)^{1/2} = \frac{1}{\alpha} \left[1 + \kappa^2 - \frac{r_s R_0^2}{(R^2 + z^2)^{3/2}} \right]^{1/2} \frac{dz}{R_0}, \quad (49)$$

and the derivative along stream lines by,

$$u^\alpha \partial_\alpha = \frac{u_p}{R_0} \frac{d}{dl} = u_p \alpha \left[1 + \kappa^2 - \frac{r_s R_0^2}{(R^2 + z^2)^{3/2}} \right]^{-1/2} \frac{d}{dz}. \quad (50)$$

From eqs. (9) and (50) we find that the change in specific energy per unit length along a given streamline is

$$\frac{d\mathcal{E}}{dl} = \frac{q^t R_0 \alpha}{\rho c^3 u_p}. \quad (51)$$

Under the assumption that the neutrino trajectories are radial we obtain

$$u_\nu q^\nu = -q^t \alpha \left\{ \gamma - u_p \left(\alpha \frac{R_0 dl}{dz} \right)^{-1} \frac{\kappa R + z}{\sqrt{R^2 + z^2}} \right\}. \quad (52)$$

Substituting the last equation into eq. (8) yields

$$\frac{ds}{dl} = \frac{q^t R_0 \alpha}{kT(\rho/m_N) u_p} \left\{ \gamma - u_p \left(\alpha \frac{dl}{dz} \right)^{-1} \frac{\kappa R + z}{\sqrt{R^2 + z^2}} \right\}, \quad (53)$$

which in the non-relativistic limit, $\gamma = \alpha = 1$, reduces to the result derived by Qian & Woosley (1996).

4.1.2. Self-similar geometry

In case of an outflow from a disk, we assume that the streamlines in the vicinity of some radius $R = R_0$ can be described by

$$(R, z) = R_0[g(\xi), \xi], \quad (54)$$

subject to the boundary condition $g(\xi = 0) = 1$. The stream function is the solution of the equation $r \sin \theta / R_0(\Psi) = g(r \cos \theta / R_0(\Psi))$. Using eq. (19) one finds

$$\left(\frac{B_p}{B_{p0}} \right)^2 = \frac{\alpha_0^2}{[\alpha_0^2 + (g_{\xi 0})^2] g^2 \alpha^2} \left\{ \frac{1 + (g_\xi)^2}{(g - \xi g_\xi)^2} - \frac{r_s}{R_0(g^2 + \xi^2)^{3/2}} \right\}, \quad (55)$$

where subscript 0 refers to the value of the corresponding quantity at the the disk midplane, viz., at $\xi = 0$, and $g_\xi = dg/d\xi$. To obtain the derivative along streamlines we note that in terms of the proper length of a given streamline, $R_0 dl = (g_{rr} dr^2 + g_{\theta\theta} d\theta^2)^{1/2}$, we have

$$u^\alpha \partial_\alpha = u_p d/dl = u_p (dl/d\xi)^{-1} d/d\xi, \quad (56)$$

with

$$(dl/d\xi)^2 = \frac{1}{\alpha^2} \left\{ 1 + (g_\xi)^2 - \frac{r_s}{R_0} \frac{(g - \xi g_\xi)^2}{(g^2 + \xi^2)^{3/2}} \right\}. \quad (57)$$

For the spherical neutrino source invoked above we obtain,

$$u_\nu q^\nu = -q^t \alpha \left\{ \gamma - u_p \left(\alpha \frac{dl}{d\xi} \right)^{-1} \frac{gg_\xi + \xi}{\sqrt{g^2 + \xi^2}} \right\}, \quad (58)$$

and

$$\frac{d\xi}{d\xi} = \frac{q^t R_0 \alpha}{\rho c^3 u_p} \frac{dl}{d\xi}, \quad (59)$$

$$\frac{ds}{d\xi} = \frac{q^t R_0}{kT(\rho/m_N) u_p} \left\{ \gamma \left(\alpha \frac{dl}{d\xi} \right) - u_p \frac{gg_\xi + \xi}{\sqrt{g^2 + \xi^2}} \right\}. \quad (60)$$

4.2. Boundary Conditions and Numerical Integration

Equations (8), (9), (13), (15)-(18), (22)-(25), and (33) have been integrated numerically for different field geometries. In each run we fix the parameters B_{p0} , $B_{\phi0}$, Ω , r_s/R_0 , R_ν/R_0 and $L_{\nu53}/R_{\nu6}^2$. In what follows, we find it more convenient to parametrize the neutrino flux in terms of the effective temperature $T_\nu \simeq 6(L_{\nu53}/R_{\nu6}^2)^{1/4}$ MeV. The temperature at the origin ($z = 0$) is determined by the condition $q^t(z = 0) = 0$, and is given to a very good approximation by $T_0 \simeq T_\nu f_{\nu n}^{1/6}$ (see eqs. [27] and [34]). The integration starts at sufficiently dense disk layers where the pressure is marginally dominated by the baryon pressure. To be more concrete, for a given T_0 the density at the origin ρ_0 was chosen such that $\sigma \lesssim 4$. The entropy per baryon at the origin is taken to be $s = 8.7 + \ln(T_{MeV}^{3/2}/\rho_0) + \sigma$ (Popham et al. 1999). The parameter η is then adjusted iteratively by changing the boundary value of the poloidal velocity u_{p0} , until a smooth transition across the slow magnetosonic point is obtained. To verify that the eigenvalue η is insensitive to ρ_0 ³, each integration has been repeated several times for a given choice of our model parameters, each time with a different value of ρ_0 . We find, indeed, that the dependence of η on ρ_0 is very weak provided that the corresponding value of σ is not too large.

5. Results

We now present solutions for the flow structure in the sub-slow region, for the two classes of field geometries described above. For the models calculated using the self-similar field geometry we invoked a parabolic field-line shape:

$$g(\xi) = 1 + \delta\xi^2, \quad (61)$$

where $0 < \delta < 1$ is an additional parameter, independent of R_0 , that controls the divergence of magnetic field lines above the disk. Note that for this choice of g $(\ln B_p)' = 0$ at $z = 0$. All the results presented below were computed using a black hole mass $M_{BH} = 3M_\odot$, and neutrinospheric radius $R_\nu = 3r_s = 10^{6.5}$ cm. For this choice of R_ν the effective temperature T_ν lies in the range 1 to 6 MeV for the range of neutrino luminosities discussed in Popham et al (1999). Sample results and the parameters employed are summarized in figs 2 - 8 and in table 1.

Typical solutions are shown in fig 2, where the change along a field line of the flow quantities indicated is plotted against the normalized height above the disk midplane, z/R_0 , for the split monopole geometry with $\kappa = 0.2$, $R_0 = R_\nu$, $B_{p0} = 10^{15}$ G, $(-B_\phi/B_p)_0 = 0.1$, and $\Omega = \Omega_k$, and for different values of the neutrino luminosity given in terms of T_ν . For each of the cases shown the temperature at the origin is $T_0 = T_\nu$ since $R_0 = R_\nu$. As seen, the slow magnetosonic point is located rather close to the disk surface, at $z \simeq R_0$, as one might expect. Well beneath the slow magnetosonic point the flow velocity is small, the density is high, and the specific entropy is dominated by the baryons, that is $\sigma \lesssim 4$. In this region the net energy deposition rate nearly vanishes, viz., $q^t \simeq 0$, and the temperature profile is given to a good approximation by equation (34). As the flow accelerates its temperature starts falling, and since the neutrino cooling rate is very sensitive to the temperature q^t increases rapidly leading to a steep rise of the entropy per baryon to its terminal value, as seen in fig 2. The reason why the energy deposition per unit length peaks well below the slow point, as seen, is that u_p there is small and, hence, the time over which a fluid element is exposed to the external neutrino flux, $dt \sim dl/u_p$, is large. Although formally the total

³The eigenvalue η should depend, to some extent, on ρ_0 through the condition $q^t(z = 0) = 0$ that fixes the the temperature at the disk layer where $\rho = \rho_0$.

energy per baryon is not conserved along streamlines, we find that it changes only slightly (to less than 0.1 %) as the flow accelerates. This is because the net energy deposited per baryon comprises only a small fraction of the baryon rest mass. The main effect of neutrino heating is not to change the net outflow energy along streamlines, but rather to enhance the baryon load by increasing the light fluid pressure in layers of higher baryon density. Thus, in practice the total energy per baryon can be considered conserved in the relativistic and mildly relativistic cases (this may not be true if the wind is highly sub-relativistic), and so the value of \mathcal{E} presents, essentially, an upper limit for the asymptotic Lorentz factor of the wind. The values of \mathcal{E} , η and the mass flux, which we somewhat arbitrarily define as $\dot{M} = \rho_0 u_{p0} 2\pi R_0^2$ (for a two-sided outflow), that corresponds to the cases depicted in fig. 2 are listed in table 1. The values of η and \mathcal{E} computed numerically are in good agreement with analytic expressions given in eqs. (46) and (47).

In fig. 3 we plotted solutions obtained for a centrifugally driven outflow along field lines in the unstable regime ($\kappa > 1/\sqrt{3}$). The effective disk surface in this example is located at $z_d = 0.1R_0$. The temperature at the surface is $T_0 = 2$ MeV, and the remaining parameters are the same as in fig. 2. As seen, the slow magnetosonic point is located very near the surface. The corresponding mass fluxes are $\dot{M}/(10^{30} \text{ gr s}^{-1}) = 7.6, 76, 95$, and 101 for $\kappa = 1, 2, 3$, and 4 , respectively. In addition to this example, we also explored other regimes of the parameter space. The main conclusion is that, quite generally, the mass loading of centrifugally driven winds from neutrino cooled disks is too large to allow acceleration to relativistic speeds. Since we are merely interested in relativistic winds here we focus, in what follows, on the regime $\kappa < 1/\sqrt{3}$.

Fig 4 exhibits the dependence of the total energy per baryon \mathcal{E} on the ratio $(-B_\phi/B_p)_0$. It is clearly seen that the magnetic energy per baryon, $\mathcal{E}_B = \mathcal{E} - 1$, depends linearly on $(-B_\phi/B_p)_0$, in agreement with the analytic expression given in eq. (47). The ratio of mass-to-magnetic flux η is found to be practically independent of $(-B_\phi/B_p)_0$. In the examples depicted in fig 4, η changes by less than 3% over the range $(-B_\phi/B_p)_0 = 10^{-3} - 1$. In fact we find that the mass flux ρu_p is highly insensitive also to the strength of the poloidal field B_{p0} , provided the Alfvén Mach number M is sufficiently small at the slow magnetosonic point (that is, $c_s \ll u_A$ there), and that it depends predominantly on the neutrino flux, the geometry of magnetic field lines, and the angular velocity Ω . This confirms that for a given choice of the latter parameters, \mathcal{E}_B is proportional to the product $(-B_p B_\phi)_0$. The results presented in fig 4 can then be readily rescaled for other choices of B_{p0} .

The dependence of baryon loading on the inclination angle of the field line is examined in fig 5, where η is plotted against the parameter κ for a fixed R_0 (which corresponds to changing the distance a in fig 1 keeping R_0 fixed). The corresponding mass flux, $\dot{M} = \rho_0 u_{p0} 2\pi R_0^2$, is indicated on the right axis. As expected, the mass flux is larger on field lines with larger inclination angles, owing to the slingshot effect. The dependence of mass loading on the radius at which the field line intersects the disk is demonstrated in fig. 6, where η and \dot{M} are plotted against R_0 for a fixed κ . As seen, the trend is that the mass flux increases with increasing R_0 . This mainly reflects the fact that the escape velocity is smaller on field lines that emanate from larger disk radii R_0 . However, the dependence is weaker than one might anticipate, owing to the decrease in the heating rate with increasing R_0/R_ν (see eq. [27] and below). We also made some runs with different values of r_s/R_ν and found the mass flux to be sensitive also to this parameter at low T_ν . General relativistic effects appear to be important near the black hole, but we do not attempt here to quantify them.

For completeness, we also examined the dependence of η on the angular velocity of magnetic flux tubes. Although the latter is naively expected to be nearly Keplerian, it is conceivable that various effects may give rise to non-Keplerian rotation of some flux tubes during certain periods. The general trend, as seen in

fig. 7, is for the baryon load to increase with increasing Ω , by virtue of the larger contribution of centrifugal forces. However, a change in Ω may also lead to a change in the Poynting flux, so the implications for the asymptotic Lorentz factor are not straightforward.

Fig 8 presents results obtained using the self-similar configuration with $g(\xi)$ given by eq. (61), for $\delta = 0.5$ (left panels) and $\delta = 0.2$ (right panels). The behavior of the solutions is rather similar to the split monopole case. We generally find low mass fluxes for which $\mathcal{E} \gg 1$ on field lines that emanate from within several r_s and that diverge not too fast at low enough neutrino temperatures ($T_\nu \lesssim 2$ MeV). We have also checked other forms of $g(\xi)$. In all cases we find that at $T_\nu \lesssim 2$ MeV relativistic outflows can be launched from the innermost disk regions.

We finally address the question whether the nuclear composition of the expelled matter changes during the acceleration of the flow. Significant evolution of the electron fraction Y_e is expected if the neutronization timescale, $t_n \simeq 10T_{MeV}^{-5}$ s, is much shorter than the outflow time $t_d = (R_0/c) \int dl/u_p$. The evolution of Y_e should take place at the base of the flow, where the temperature is highest and, hence, t_n is shortest, and where u_p is smallest and, hence, t_d is longest. For most cases studied above we find the outflow time to be comparable to t_n , and so the n/p ratio is expected to evolve during the initial acceleration phase. Quantitative treatment of the nuclear processes in the wind is beyond the scope of this paper and is left for a future investigation.

6. Conclusions

We have explored stationary, axisymmetric GRMHD disk outflows in Schwarzschild geometry with neutrino-driven mass ejection, under conditions anticipated in hyperaccreting black holes. We have examined the dependence of mass loading of the outflow on the neutrino luminosity emitted by the disk and on other wind quantities, for a range of effective neutrino temperatures $T_\nu = 1 - 6$ MeV, which for the simplified geometry of the neutrino emission zone invoked in our model corresponds to a neutrino luminosity range $L_\nu = 10^{51} - 10^{53}$ erg s $^{-1}$. We find that up to a few percent of the neutrino luminosity produced inside the disk is deposited at the upper disk layers and used up to eject baryons along magnetic field lines. The neutrino-driven mass flux depends predominantly on the effective neutrino temperature at the base of the flow, on magnetic field geometry in the sub-slow magnetosonic region, and on the angular velocity of magnetic flux surfaces, but is highly insensitive to the strength of poloidal and toroidal magnetic field components near the surface provided the Alfvén Mach number is sufficiently small at the slow point; the dependence on neutrino luminosity and the shape of magnetic field lines near the disk surface appears to be particularly sensitive. The heating of the wind by the escaping neutrinos results in a steep rise of the entropy per baryon, s , during the initial acceleration phase, after which it saturates. The final value of s is larger for lower L_ν , but does not seem to reach extreme values. For the range of conditions explored above it is typically below $100k_B$ per baryon.

Our principle conclusion is that ejection of relativistic outflows from the innermost disk radii, within several r_s or so, is possible in principle for certain magnetic field configurations even in non-rotating black holes, provided the neutrino luminosity is sufficiently low, and the magnetic field is sufficiently strong. In the case of the split monopole field delineated in section 4.1, we obtain a mass flux of $\rho u_p \sim 10^{14}$ gr cm $^{-2}$ s $^{-1}$ on field lines in the vicinity of the innermost stable circular orbit that make an angle $\tilde{\theta} \sim 12^\circ$ with the rotation axis, for a neutrino luminosity $L_\nu \sim 10^{52}$ erg s $^{-1}$ (corresponding to $T_\nu \sim 2$ MeV). The outflow along those field lines can, therefore, accelerate to Lorentz factors $\gamma_\infty \lesssim 100$ if the magnetic field strength at

the disk surface is $B_{p0} \sim 10^{15}$ G. The mass flux depends sensitively on both $\tilde{\theta}$ and T_ν , as can be seen from figure 5 and table 1, and so a steep profile of the Lorentz factor across the polar jet is naively expected. We find a similar trend also for the other field geometries adopted. Thus, the picture often envisioned, of an ultra-relativistic core surrounded by a slower, baryon rich wind (e.g., Levinson & Eichler 1993, 2000;) seems a natural consequence of neutrino-assisted MHD disk outflows. At higher effective temperatures, $T_\nu > 2$ MeV or so, the baryon load is typically well in excess of the value inferred in GRB fireballs, and the wind is expected to be slow. This conclusion may be altered if the central black hole is rapidly rotating.

The hyperaccretion process is likely to be intermittent, leading to temporal changes in the neutrino luminosity. This should result in large variations of the Lorentz factors of consecutive fluid shells expelled from the disk in the polar region, owing to the sensitive dependence of mass loading on L_ν . In this situation we expect strong shocks to form in the outflow. If the polar disk outflow is associated with the GRB-producing jet, then the observed gamma-ray emission can be quite efficiently produced behind those shocks.

It is worth noting that the conditions we find to be optimal for launching an ultrarelativistic jet in the polar region, are also the conditions favorable for large neutron-to-proton ratio in the disk. For example, by employing the results presented in table 2 of Popham et al. (1999), we estimate $T_\nu < 2$ MeV for accretion rates $\dot{M}_{acc} \lesssim 0.1 M_\odot$ s⁻¹ into a $3 M_\odot$ Schwarzschild black hole. Under such conditions a neutron-to-proton ratio larger than 10 is expected inside the disk within a few r_s for viscosity parameters $\alpha < 0.03$ (Pruet et al. 2003; see also Beloborodov 2003). If turbulent mixing can quickly lift up neutron rich matter to the surface layers, then it can be picked up by the outflow. Beloborodov (2003) has shown that deneutronization is not expected at temperatures below about 8 MeV if the mixing timescale is of the order of Ω_k^{-1} . However, because at low T_ν the flow time is comparable to the neutronization timescale, the electron fraction Y_e may evolve as the flow accelerates and the final nuclear composition of the outflow may somewhat change. Further analysis is needed to determine the wind composition, but the trend seems to be that ultrarelativistic disk outflows can plausibly contain neutron rich matter. This is in accord with the conjecture often made, that fireballs pick up neutron rich material from the disk.

I thank Arieh Konigle for inspiring conversations, the referee Nektarios Vlahakis for useful comments, and Jason Pruet for helpful correspondence. This work was supported by an ISF grant for the Israeli Center for High Energy Astrophysics

A. Equation of Motion for General Relativistic, Neutrino-Assisted MHD Wind

The projection of the momentum equation on the poloidal direction yields eq. (15). We can equivalently derive this equation by differentiating eq. (14) along a given streamline $\Psi = \text{const}$ (e.g., Camenzind 1986). To simplify the notation let us denote

$$k_0 = \alpha^2 - R^2\Omega^2, \quad (\text{A1})$$

$$k_2 = (\mathcal{E} - \Omega\mathcal{L})^2, \quad (\text{A2})$$

$$k_4 = \frac{\mathcal{L}^2}{R^2} - \frac{\mathcal{E}^2}{\alpha^2}. \quad (\text{A3})$$

Differentiating the above equations along a stream line, making use of the fact that η , Ω and \mathcal{L} are conserved on magnetic surfaces, yields

$$(k_0)' = 2\alpha^2(\ln \alpha)' - 2R^2\Omega^2(\ln R)', \quad (\text{A4})$$

$$(k_2)' = 2(\mathcal{E} - \Omega\mathcal{L})\mathcal{E}', \quad (\text{A5})$$

$$(k_4)' = \frac{2\mathcal{E}^2}{\alpha^2}(\ln\alpha)' - 2\frac{\mathcal{L}^2}{R^2}(\ln R)' - 2\frac{\mathcal{E}^2}{\alpha^2}(\ln\mathcal{E})'. \quad (\text{A6})$$

Taking the enthalpy to be a function of the density ρ and the entropy per baryon s we further obtain,

$$(\ln h)' = a_s^2(\ln\rho)' + \frac{\partial \ln h}{\partial \ln s}(\ln s)', \quad (\text{A7})$$

$$(\ln M^2)' = (\ln h)' - (\ln\rho)' = (a_s^2 - 1)(\ln\rho)' + \frac{\partial \ln h}{\partial \ln s}(\ln s)', \quad (\text{A8})$$

where $a_s^2 = (\partial \ln h / \partial \ln \rho)_s$ is the adiabatic sound speed. Upon differentiating eq. (14) along a stream line, using the above results together with eqs. (25) and (26), we arrive at

$$(\ln u_p)' = (N + N_q)/D, \quad (\text{A9})$$

where the terms in the nominator are given by

$$N = \zeta_1(\ln B_p)' + \zeta_2(\ln\alpha)' + \zeta_3(\ln R)', \quad (\text{A10})$$

with

$$\zeta_1 = -(k_0 - M^2)^2 \left[(1 + u_p^2)(k_0 - M^2)c_s^2 - M^2 \frac{B_\phi^2}{4\pi h\rho} \right], \quad (\text{A11})$$

$$\zeta_2 = \frac{1}{h^2(1 - a_s^2)} \left\{ \frac{M^6\mathcal{E}^2}{\alpha^2} - \left(3\mathcal{E}^2 - \frac{R^2\Omega^2\mathcal{E}^2}{\alpha^2} - \frac{2\mathcal{L}^2}{R^2} \right) M^4 + \alpha^2 k_2(3M^2 - k_0) \right\}, \quad (\text{A12})$$

$$\zeta_3 = \frac{1}{h^2(1 - a_s^2)} \left\{ -\frac{\mathcal{L}^2}{R^2} M^6 + \left(3\mathcal{L}^2\Omega^2 - \frac{\alpha^2\mathcal{L}^2}{R^2} - \frac{2R^2\Omega^2\mathcal{E}^2}{\alpha^2} \right) M^4 - R^2\Omega^2 k_2(3M^2 - k_0) \right\}, \quad (\text{A13})$$

and

$$N_q = \zeta_4(\ln\mathcal{E})' + \zeta_5(\ln s)', \quad (\text{A14})$$

with

$$\zeta_4 = \frac{1}{h^2(1 - a_s^2)}(k_0 - M^2)[(k_0 - 2M^2)(\mathcal{E} - \Omega\mathcal{L})\mathcal{E} + M^4\mathcal{E}^2/\alpha^2], \quad (\text{A15})$$

$$\zeta_5 = \frac{(5 + 8\sigma)}{(5 + 10\sigma + 2\sigma^2)} \frac{sc_s^2}{h^2} [k_4 M^6 - k_2(k_0^2 - 3k_0 M^2 + 3M^4)], \quad (\text{A16})$$

and the denominator by

$$D = (\alpha^2 - R^2\Omega^2 - M^2)^2 \left[(u_p^2 - c_s^2)(\alpha^2 - R^2\Omega^2 - M^2) + M^2 \frac{B_\phi^2}{4\pi h\rho} \right]. \quad (\text{A17})$$

In terms of the slow and fast magnetosonic speeds,

$$u_{SM}^2 = K - \sqrt{K^2 - c_s^2 u_A^2 (\alpha^2 - R^2\Omega^2)}, \quad (\text{A18})$$

$$u_{FM}^2 = K + \sqrt{K^2 - c_s^2 u_A^2 (\alpha^2 - R^2\Omega^2)}, \quad (\text{A19})$$

where

$$K = \frac{1}{2} \left[(\alpha^2 - R^2\Omega^2)u_A^2 + c_s^2 + \frac{B_\phi^2}{4\pi h\rho} \right], \quad (\text{A20})$$

the denominator D can be rewritten as in eq. (16).

REFERENCES

Bachall, J. N., & Meszaros, P. 2000, Phys. Rev. Lett., 85, 1362

Beloborodov, A.M. 2003, ApJ, 588, 931

Bethe, H. & Wilson, J. R. 1985, Ap.J. 295, 14

Blandford, R.D., & Payne, D.G. 1982, M.N.R.A.S., 199, 883

Camenzind, M. 1986, A&A, 162, 32

Contopoulos, J. 1994, ApJ, 432, 508

Derishev, E.V., Kocharyan, V.V., & Kocharyan, V.I. 1999, ApJ, 521, 640

Duncan, R. C., Shapiro, S. L., & Wasserman, I. 1986, ApJ, 309, 141

Fuller, G. M., Pruet, J. & Abazajian, K. 2000, Phys. Rev. Lett., 85, 2673

Goodman, J., Dar, A., and Nussinov, S. 1987, ApJ, 314, L7

Levinson, A. 2005, in “Trends in Black Hole Research”, New York, Nova Science Publishers, 125-156

Levinson, A., & Eichler, D. 1993, ApJ, 418, 386

Levinson, A., & Eichler, D. 2000, Phys. Rev. Lett., 85, 236

Li, Z.-Y., Chiueh, T. & Begelman, M.C. 1992, ApJ, 394, 459

McKinney, J. C., 2005, astro-ph/0506369

McKinney, J. C., 2005b, ApJ, 630, L5

Meszaros, P., & Rees, M. J. 1997, ApJ, 482, L29

Popham, R. Woosley, S.E., & Fryer, F., 1999, ApJ, 518, 356

Proga, D. & Begelman, M.C. 2003, ApJ, 592, 767

Proga, D. MacFadyen, A.I., Armitage, P.J. & Begelman, M.C. 2003, ApJ, 599, L5

Pruet, J., Woosley, S.E., & Hoffman, R.D. 2003, ApJ, 586, 1254

Pruet, J., Thompson, T. A., & Hoffman, R. D. 2004, ApJ, 606, 1006

Pruet, J., Woosley, S. E., Buras, R., Janka, H.-T., & Hoffman, R. D. 2005, ApJ, 623, 325

Ogilvie, G. I. 1997, MNRAS, 288, 63

Qian, Y.-Z. & Woosley, S.E., 1996, ApJ, 471, 331

Rossi, E. M., Beloborodov, A. M. & Rees, M. J. 2005, astro-ph/0512495

Rosswog, S., & Ramirez-Ruiz, E. 2003, MNRAS, 343, L36

Takahashi, M., Nita, S., Tatematsu, Y., & Tominatsu, A. 1990, ApJ, 363, 206

Thompson, T. A., Burrows, A. & Meyer, B. S. 2001, ApJ, 562, 887

Van Putten, M.H.P.M. & Levinson, A. 2003, ApJ, 584, 937

Vlahakis, N., Peng, F. & Konigl, A. 2003, ApJ, 594, L23

Vlahakis, N. & Konigl, A. 2003, ApJ, 596, 1080

Witti, J., Janka, H.-T., & Takahashi, K 1994, A&A, 286, 841

Woosley, S. E., Wilson, J. R., Mathews G. J., Hoffman, R. D., & Meyer, B. S. 1994, ApJ, 433, 229

Table 1: Numerical models

Model ^a	(κ, δ) ^b	R_0/r_s	R_0/R_ν	$L_{\nu 53}/R_{\nu 6}^2$	T_ν MeV	T_0 MeV	η gr cm $^{-2}$ s $^{-1}$ G $^{-1}$	\dot{M} 10 30 gr s $^{-1}$	s_∞ ^c	\mathcal{E}
SM1...	0.2	3	1	0.012	2	2	0.18	0.011	44	492
SM2...	0.2	3	1	0.062	3	3	7.4	0.47	32	13
SM3...	0.2	3	1	0.197	4	4	116	7.4	29	1.8
SM4...	0.1	3	1	0.012	2	2	0.028	0.0018	87	3100
SM5...	0.1	3	1	0.197	4	4	22	1.39	55	5.1
SM6...	0.3	3	1	0.012	2	2	1.6	0.1	19	50
SM7...	0.3	3	1	0.197	4	4	1368	86.6	15	1.03
SM8...	0.2	9	3	0.012	2	1.25	0.37	0.024	18	161
SM9...	0.2	9	3	0.197	4	2.5	396	25	15	1.1
SS1...	0.5	3	1	0.012	2	2	26.4	1.67	14	4.3
SS2...	0.5	3	1	0.062	3	3	1008	64	13	1.05
SS3...	0.2	3	1	0.012	2	2	0.29	0.018	29	309
SS4...	0.2	3	1	0.062	3	3	313	19.8	13	1.2

^a “SM” stands for split monopole geometry, “SS” for self-similar geometry.

^b The numerical values in this column correspond to values of κ in the “SM” models, and to values of δ in the “SS” models (see text for further details).

^c s_∞ refers to the asymptotic value of the dimensionless entropy per baryon s .

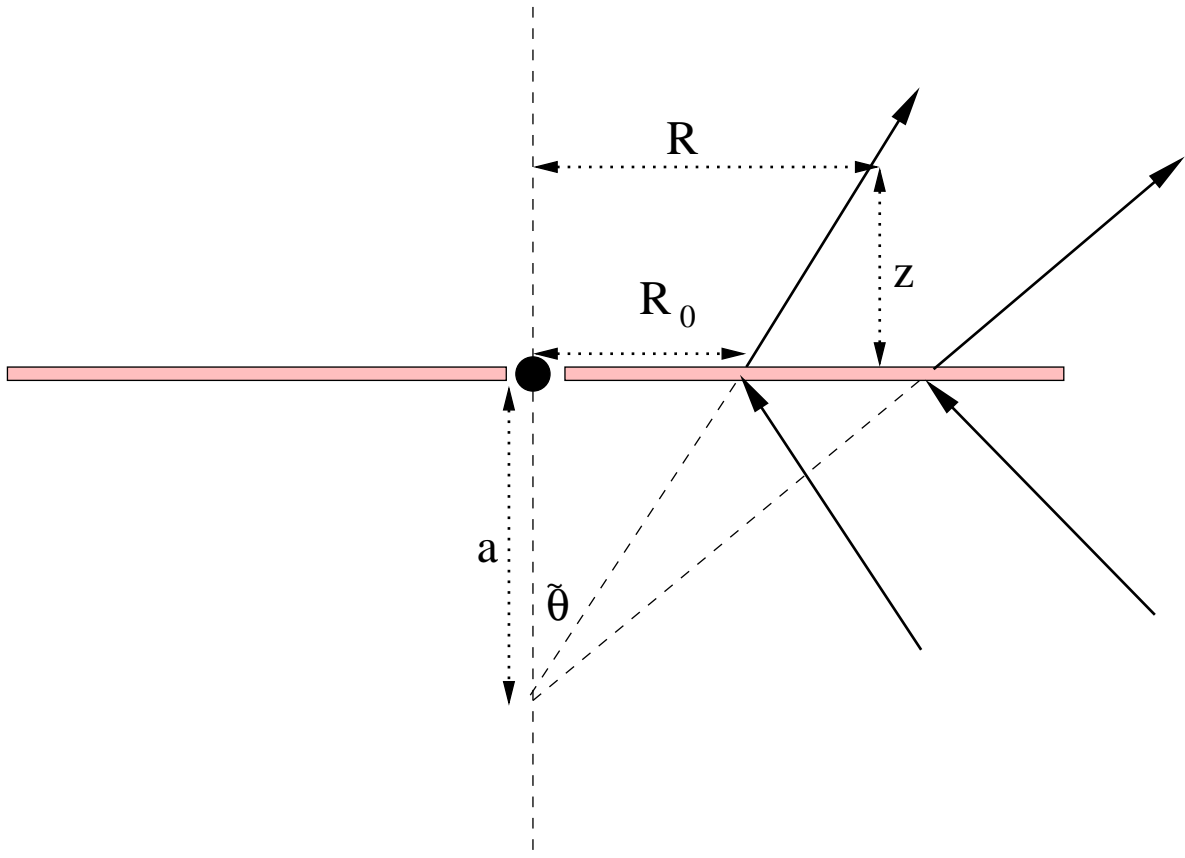


Fig. 1.— Sketch of the split monopole configuration employed for the numerical computations. The origin of the monopole is shifted a distance a from the black hole along the symmetry axis of the system. The magnetic field is supported by a current sheet in the equatorial plane. The field line parameter is defined as $\kappa = \tan \tilde{\theta}$. The radius R_0 at which the field line meets the disk is indicated.

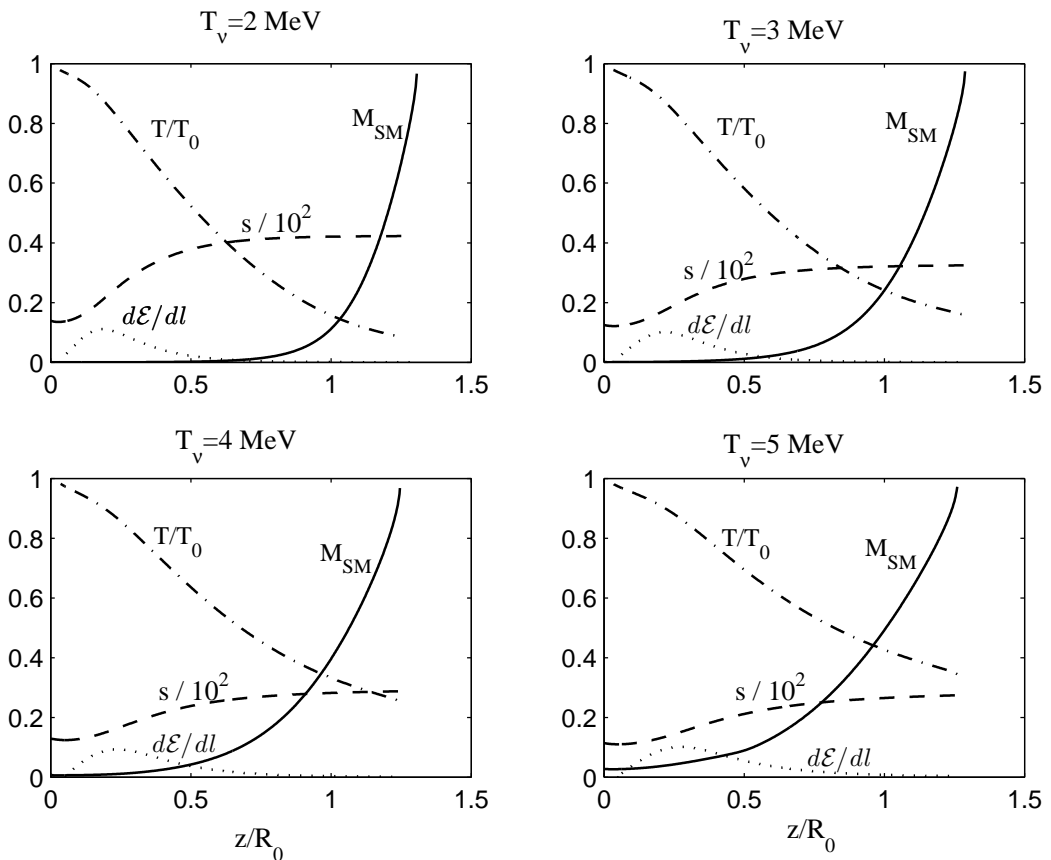


Fig. 2.— Profiles of various quantities in the sub-slow magnetosonic region, computed using the split monopole magnetic field of fig. 1 with $\kappa = 0.2$, $B_{p0} = 10^{15}$ G, $(-B_\phi/B_p)_0 = 0.1$, and Keplerian rotation, viz., $\Omega = \Omega_k$. Each panel corresponds to a run with a different neutrino luminosity (indicated in terms of the effective temperature T_ν ; see text for details). The quantities plotted in each panel are: the slow magnetosonic speed M_{SM} (solid line), the dimensionless temperature T/T_0 (dashed line), the dimensionless energy density $s/10^2$ (dash-dot line), and the derivative dE/dl (dotted line).

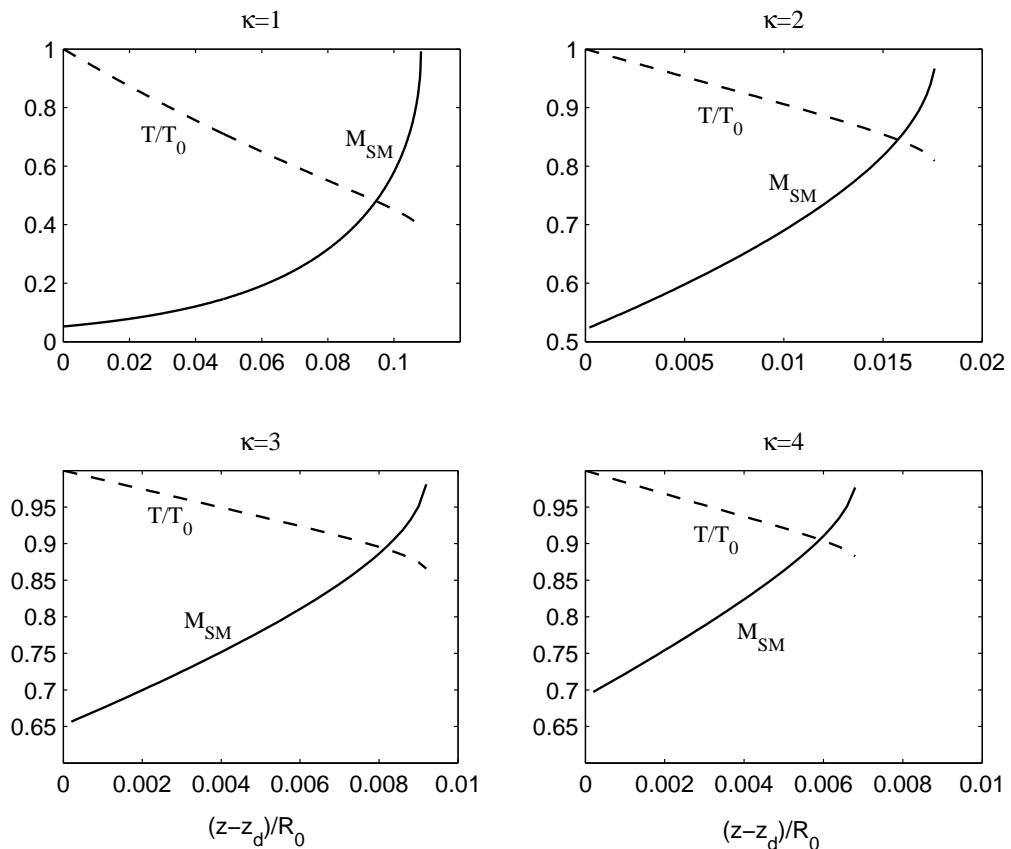


Fig. 3.— Profiles of T/T_0 and M_{SM} for centrifugally driven outflows. The surface temperature in all cases shown is $T_0 = 2$ MeV, and the remaining parameters are the same as in fig. 2.

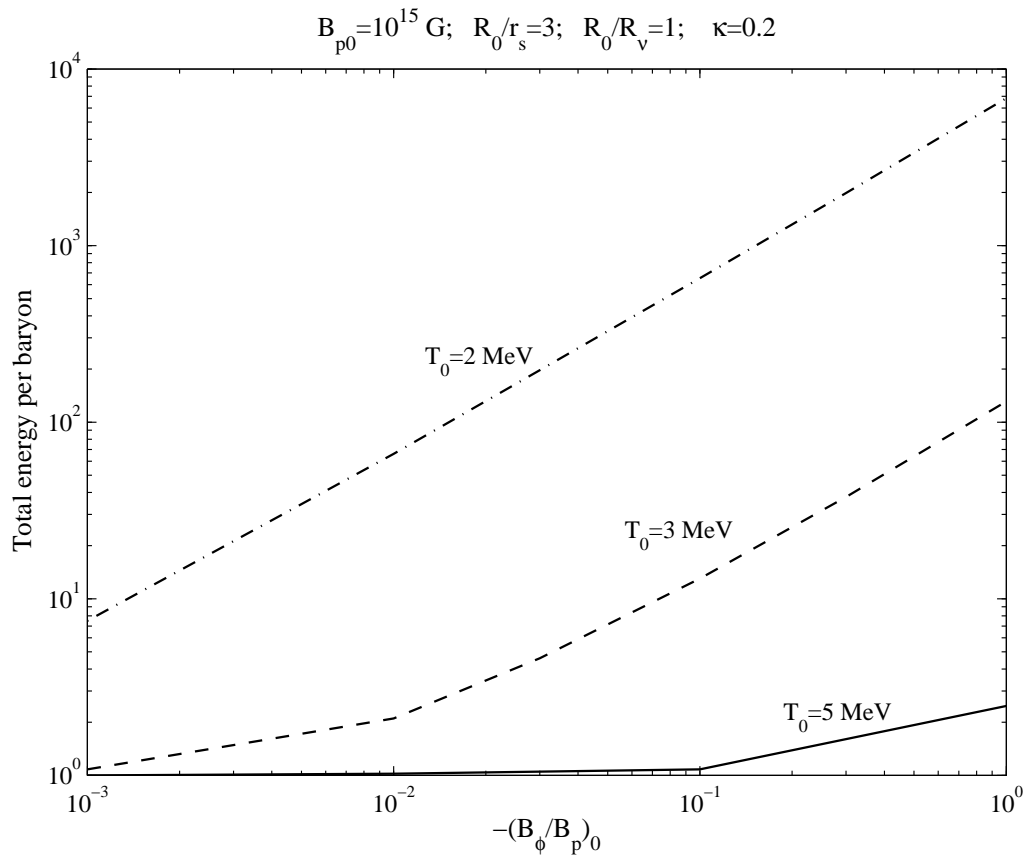


Fig. 4.— Total energy per baryon, \mathcal{E} , versus the ratio of the toroidal and poloidal components of the magnetic field at the disk surface, $-(B_\phi/B_p)_0$.

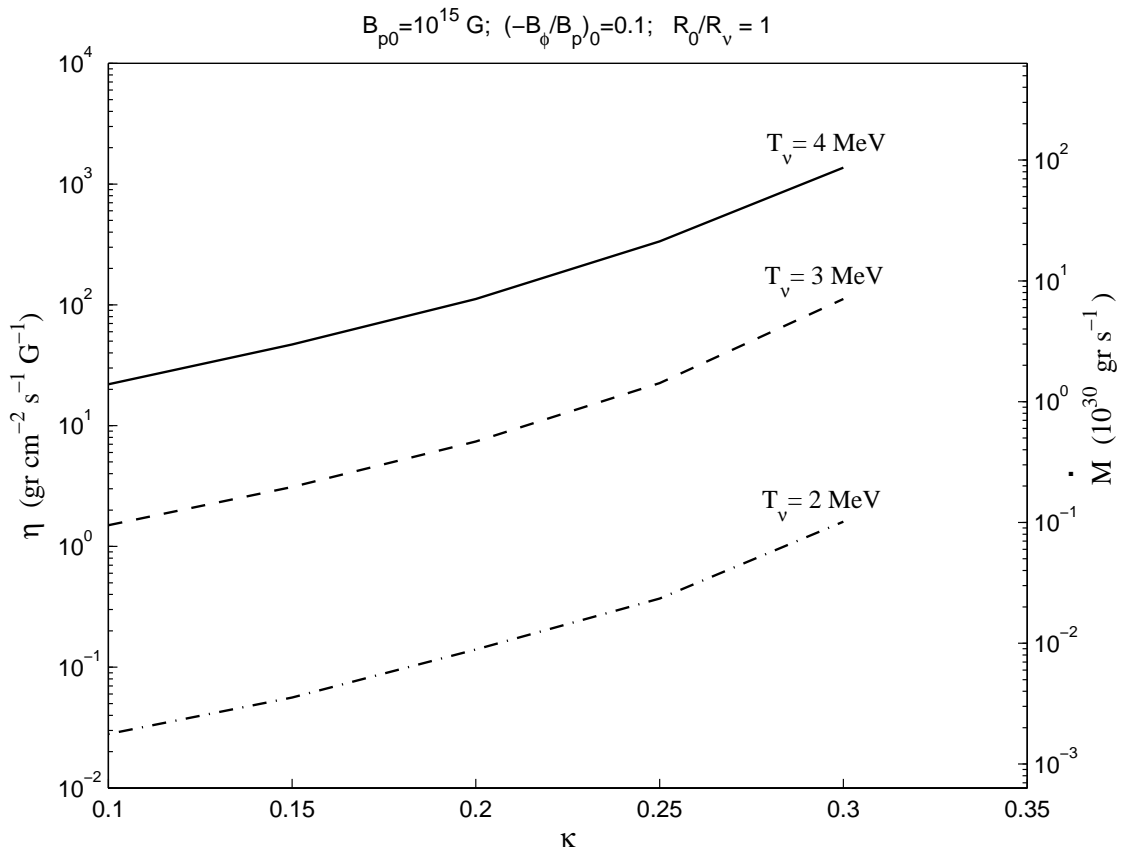


Fig. 5.— Mass-to-magnetic flux ratio η (left axis) as a function of the split-monopole field line parameter κ . The corresponding values of the mass flux \dot{M} , as defined in the text, are indicated on the right axis.

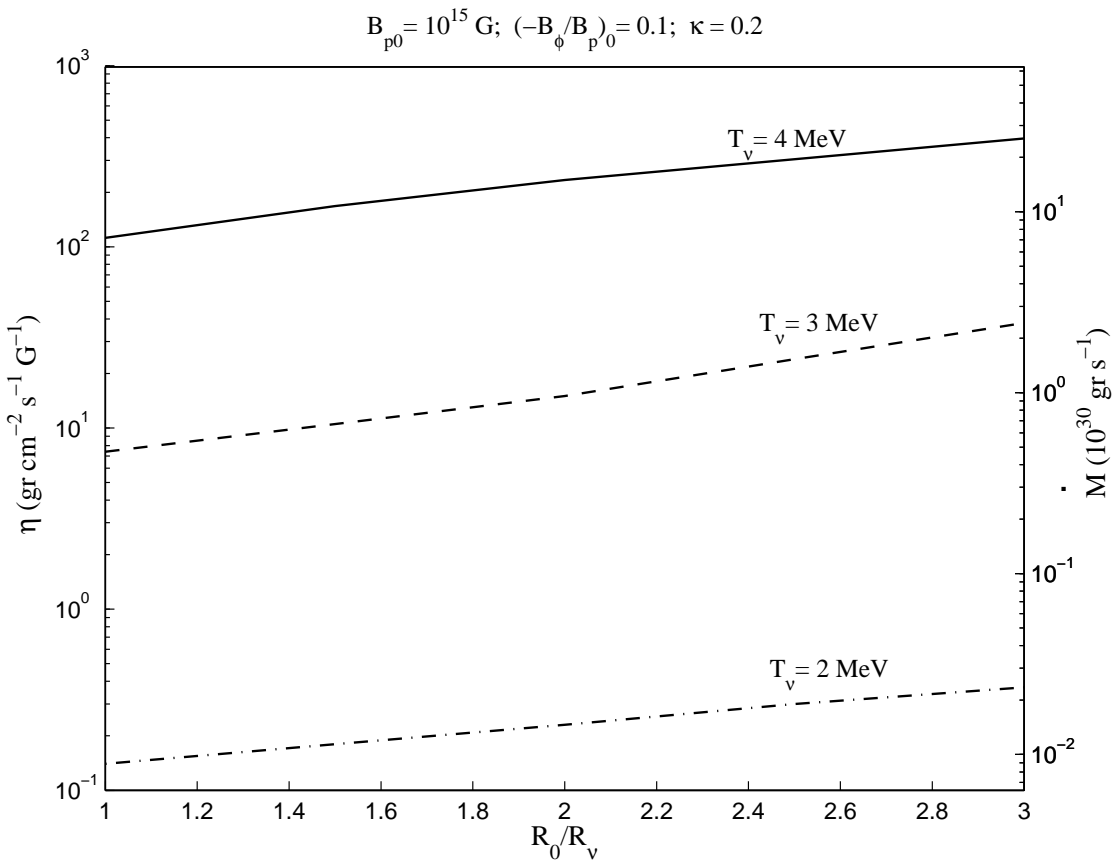


Fig. 6.— The dependence of η and \dot{M} on the radius R_0 at which the field line intersects the disk (see fig. 1). The distance a in fig. 1 is adjusted such that κ is kept fixed as R_0 is varied

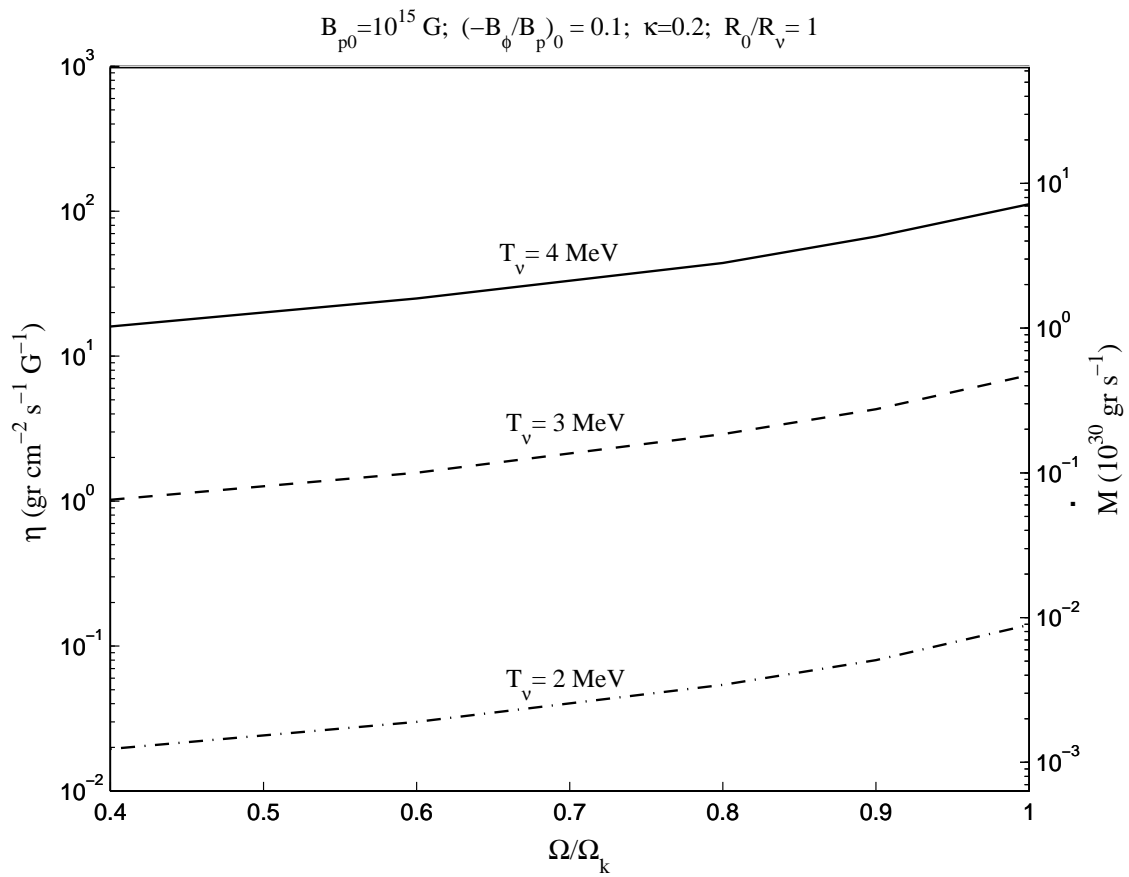


Fig. 7.— η and \dot{M} versus angular velocity of the field line, Ω , given in units of the Keplerian angular velocity at the disk midplane Ω_k .

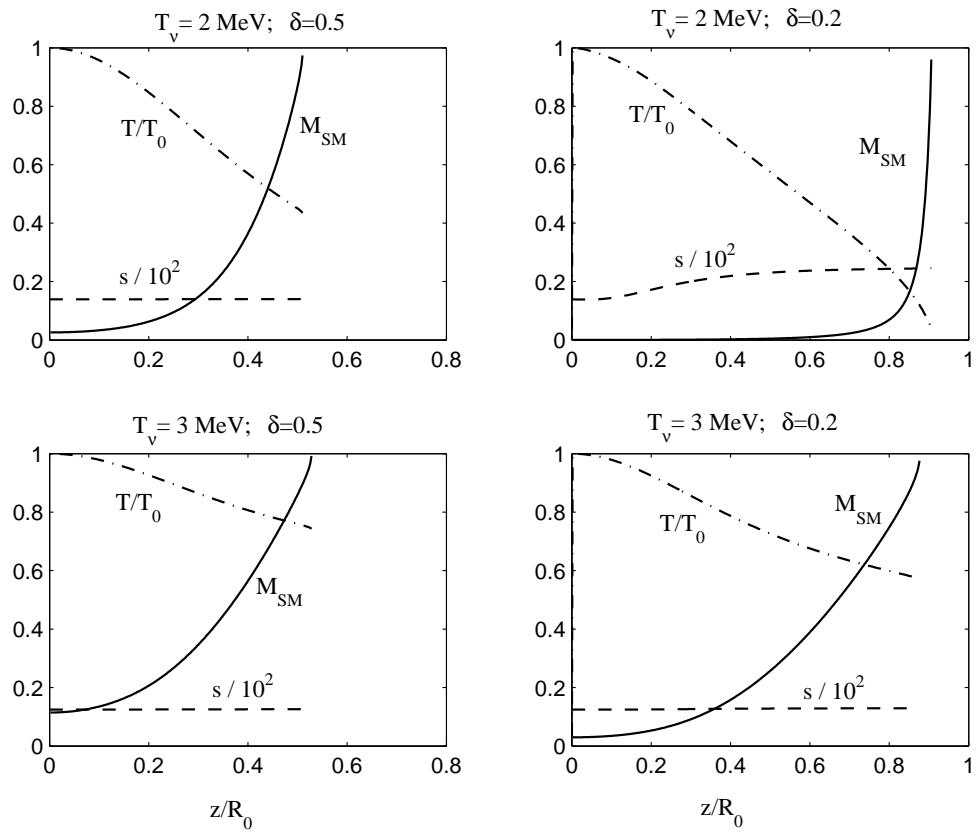


Fig. 8.— Same as fig. 2, but for a self-similar geometry with the parabolic field lines given in eq. (61).